Regular Article - Living Systems

Analytical investigation of compartmental models and measure for reactions of governments

Yahya Öz[a]

Department of Research and Technology Centers, R&D and Technology Directorate, Turkish Aerospace, 06980 Ankara, Turkey

Abstract The ongoing coronavirus disease 2019 (COVID-19) pandemic poses a major threat to the worldwide health care. In this context, epidemic modelling is an integral part of containment strategies. Compartmental models are typically used for this purpose. Analytical solutions of the two distinct but connected Susceptible-Infectious-Recovered-Deceased (SIRD) and Susceptible-Infectious-Quarantine-Recovered (SIQR) models are presented in this study. Furthermore, the behaviour at the start of a disease outbreak is derived. This analysis shows that a combination of transmission, recovery and isolation rates dominates the behaviour at the start of an epidemic. In addition, the loss occurring due to quarantine and lockdown measures is investigated, where it can be observed that quarantine procedures lead to a smaller loss in comparison with lockdown regulations. Within this framework, optimized strategies that lead to a constant epidemic peak or a minimized loss are presented.

1 Introduction

Since December 2019, a total of 499748065 many infections and 6181560 many deaths due to the ongoing COVID-19 pandemic were confirmed until April 12, 2022 [1]. Therefore, biological modelling of such disease outbreaks plays an essential role in containing these and possible other epidemics or pandemics. Such models allow the study of infection dynamics and offer the possibility of assessing the potential consequences of various options for population or government reactions and thus developing a strategy that is optimized as well as feasible.

Studying epidemics by use of compartmental models, which are deterministic mean-field models, is a well-established academic discipline [2–5]. The Susceptible-Infectious-Removed (SIR) model is a basic model [6] that assumes that the total population can be divided into three classes: susceptible, infected and removed population parts. Note that within this approach demographic effects are neglected since infection dynamics are often much faster than demographic dynamics. Infections occur due to contact between infected and susceptible individuals. The number of infected individuals decreases due to treatment, quarantine measures and death cases.

In addition, variations of the SIR model like SIRD and SIQR models and also their modified versions exist [7–20]. On the one hand, the SIRD model considers the number of susceptible, infected, recovered, and dead

people. Correspondingly, a susceptible individual in contact with an infected person is likely to get infected. This individual can either recover from the disease or die. Hence, the sum of susceptible, infected, recovered, and dead remains constant. Furthermore, it is conjectured that all individuals who are exposed to the disease get infected instantly. Thus, no latent time between exposure and infection exists within this model. In addition, confinement or quarantine measures are neglected. On the other hand, the SIQR model is a compartmental model which describes a population by four compartments, assuming the existence of an additional compartment of quarantined individuals in contrast to the SIR model. In common epidemics, only symptomatic patients are considered as infectious and the quarantine measure is launched to remove symptomatic individuals from the population. Nonetheless, infectious diseases like COVID-19 also yield pre-symptomatic and asymptomatic patients who are infectious and thus are also considered as part of the additional compartment.

Remarkably, due to the COVID-19 pandemic modelling and simulation is of great prominence. Many important results were summarized in [6,21]. The SIR model, introduced in [5], was used for the purpose of studying the COVID-19 outbreak [22,23], while the SIRD model was also studied for the analysis of the pandemic [24,25].

Therefore, analytical results are derived for the SIRD and SIQR cases in Sects. 2.1–2.4. These formulae (describing the epidemic peak, analytical solutions for

[a] e-mail: yahyaoz@metu.edu.tr (corresponding author)

all times t and the small time limit) are obtained trivially by considering well-known expressions for the SIR model. In addition, a novel analysis of the daily new cases is presented in Sect. 2.5.

Moreover, the loss due to reactions of government and population is investigated by use of novel measure and loss functions. Two different strategies are presented. On the one hand, the epidemic peak is kept constant. On the other hand, the loss is minimized with regard to a given measure. This analysis is crucial since drastic measures were taken for the purpose of containing the spread of COVID-19. However, a major burden of the COVID-19 outbreak and a worldwide recession is observable [26,27].

2 Results obtained by use of the connection between compartmental models

2.1 SIR, SIRD and SIQR models

Within the framework of compartmental models, SIR [28–33], SIRD [34–36] and SIQR [37–40] approaches are well-known methods for the purpose of studying epidemic disease outbreaks. These models are given by sets of ordinary differential equations that describe the dynamics of the outbreak by rate equations. The SIR model is given by

$$\frac{\mathrm{d}}{\mathrm{d}t}s_1(t) = -\beta s_1(t) i_1(t), \tag{1a}$$

$$\frac{\mathrm{d}}{\mathrm{d}t}i_1(t) = \beta s_1(t) i_1(t) - \gamma i_1(t), \tag{1b}$$

$$\frac{\mathrm{d}}{\mathrm{d}t}r_1(t) = \gamma i_1(t), \tag{1c}$$

while the SIRD model is characterized by

$$\frac{\mathrm{d}}{\mathrm{d}t}s_2(t) = -\beta s_2(t) i_2(t), \tag{2a}$$

$$\frac{\mathrm{d}}{\mathrm{d}t}i_2(t) = \beta s_2(t) i_2(t) - (\gamma + \sigma) i_2(t), \tag{2b}$$

$$\frac{\mathrm{d}}{\mathrm{d}t}r_2(t) = \gamma i_2(t), \tag{2c}$$

$$\frac{\mathrm{d}}{\mathrm{d}t}d_2(t) = \sigma i_2(t) \tag{2d}$$

and the SIQR model is described by

$$\frac{\mathrm{d}}{\mathrm{d}t}s_3(t) = -\beta s_3(t) i_3(t), \tag{3a}$$

$$\frac{\mathrm{d}}{\mathrm{d}t}i_3(t) = \beta s_3(t) i_3(t) - (\gamma + \delta) i_3(t), \tag{3b}$$

$$\frac{\mathrm{d}}{\mathrm{d}t}q_3(t) = \delta i_3(t) - \mu q_3(t), \tag{3c}$$

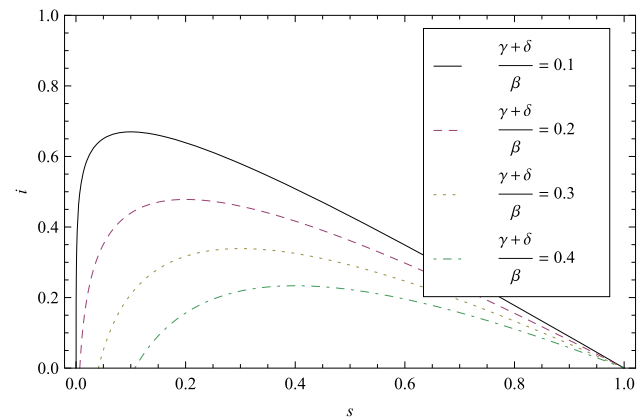$$\frac{\mathrm{d}}{\mathrm{d}t}r_3(t) = \gamma i_3(t) + \mu q_3(t), \tag{3d}$$

Fig. 1 Fraction of infected individuals i_3 depending on the fraction of susceptible individuals s_3 for $\frac{\gamma+\delta}{\beta} = 0.1, 0.2, 0.3, 0.4$

where t is the time, β the transmission rate, γ the recovery rate of infectious individuals, δ the isolation rate, σ the mortality rate, and μ the recovery rate of isolated individuals. Remarkably, these parameters are measurable quantities during an outbreak. Isolation rate δ and transmission rate β depend on government reactions to an outbreak, while β also depends on population reactions. The functions $s_j(t)$, $i_j(t)$, $q_j(t)$, $r_j(t)$ and $d_j(t)$, $j = 1, 2, 3$ with accordingly chosen j, describe the fractions of susceptible, infectious, isolated, removed (deceased or recovered for SIR and SIQR while only recovered for SIRD) and deceased individuals within the total population N at time t. Thus, $s_1(t) + i_1(t) + r_1(t) = 1$, $s_2(t) + i_2(t) + r_2(t) + d_2(t) = 1$ and $s_3(t) + i_3(t) + q_3(t) + r_3(t) = 1$ hold. Note that the initial data of the functions $s_j(t)$ is represented by $s_j(0)$ for $j = 1, 2, 3$. Typically, $s_j(0) = 1 - \frac{1}{N}$ is used since it can be assumed that one infected individual exists in a community at the start of an epidemic outbreak.

2.2 Epidemic peak

Dividing Eq. (3b) with Eq. (3a) in the SIQR model and integrating over s_3 leads to

$$i_3(s_3(t)) = 1 - s_3(t) + \frac{\gamma + \delta}{\beta} \ln s_3(t), \tag{4}$$

which describes the fraction of infected individuals in the (s_3, i_3) plane for the SIQR model. In analogy, setting the isolation rate $\delta = 0$ ($\delta = \sigma$) and changing the index $3 \rightarrow 1$ ($3 \rightarrow 2$) yields the equation describing the fraction of infected individuals in the (s_1, i_1) ((s_2, i_2)) plane for the SIR (SIRD) model. The (s_3, i_3) plane is depicted in Fig. 1 for varying $\frac{\gamma+\delta}{\beta}$.

The peak of this plane increases for increasing transmission rate β or decreasing $\gamma + \delta$ and lies at position
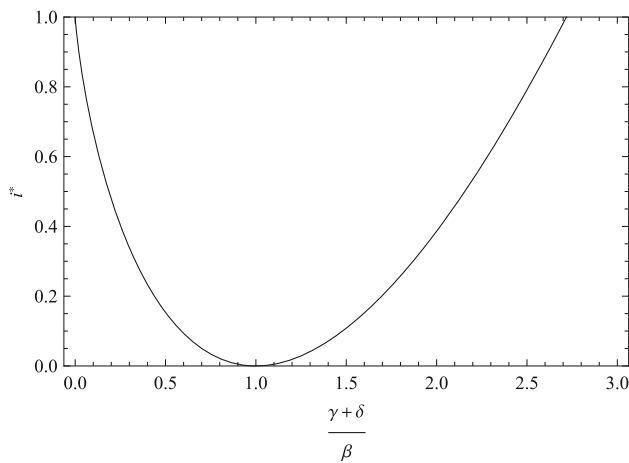
Fig. 2 Epidemic peak i_3^* depending on $\frac{\gamma+\delta}{\beta}$

(s_3^*, i_3^*),

$$s_3^* = \frac{\gamma+\delta}{\beta}, \qquad i_3^* = 1 + \frac{\gamma+\delta}{\beta}\left(\ln\frac{\gamma+\delta}{\beta} - 1\right). \quad (5)$$

The epidemic peak i_3^* is depicted in Fig. 2. It shows a minimum at $\beta = \gamma + \delta$ while increasing transmission rate β or decreasing $\gamma + \delta$ yield increasing i_3^* for $\beta > \gamma + \delta$. Contrarily, for $\beta < \gamma + \delta$ decreasing transmission rate β or increasing $\gamma+\delta$ increases i_3^*. For $\frac{\gamma+\delta}{\beta} > \mathrm{e}$ (with Euler's number e) the peak i_3^* is larger than 1, which is prohibited in the framework of the SIQR model.

2.3 Exact results

Exact results for the SIR model are well-known [41–43] and given by

$$s_1(t) = s_1(0)\,u_1(t), \quad (6a)$$

$$i_1(t) = 1 + \frac{\gamma}{\beta}\ln u_1(t) - s_1(0)\,u_1(t), \quad (6b)$$

$$r_1(t) = -\frac{\gamma}{\beta}\ln u_1(t), \quad (6c)$$

where the function $u_1(t)$ is defined by

$$t = \int_1^{u_1(t)} \frac{\mathrm{d}\xi}{\xi\left(\beta\xi s_1(0) - \beta - \gamma\ln\xi\right)}. \quad (6d)$$

These solutions are depicted in Fig. 3.

The SIRD model reduces to the SIR model by use of $\frac{\mathrm{d}}{\mathrm{d}t}\left(r_2(t) + d_2(t)\right) = \frac{\mathrm{d}}{\mathrm{d}t}r_1(t)$, changing the index $2 \to 1$ and setting the mortality rate $\sigma = 0$. Hence, Eqs. (6a), (6b) and (6d) also hold for the SIRD case if the replacements in the indices $1 \to 2$ are performed while Eq. (6c) is a solution for $r_1(t) = r_2(t) + d_2(t)$. Hence, exact solutions are given by

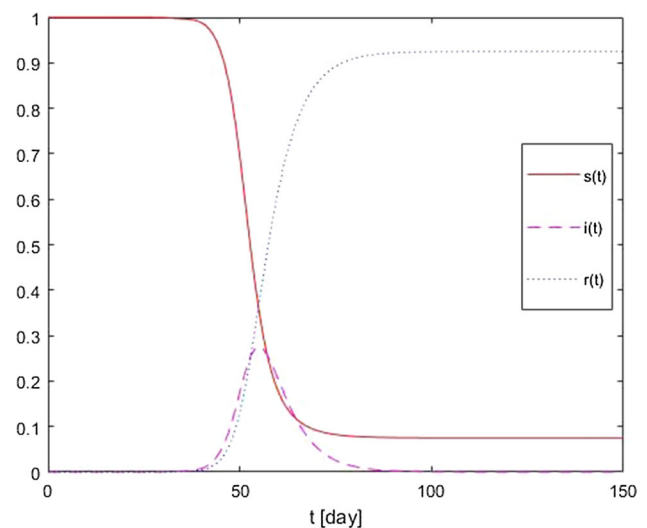$$s_2(t) = s_2(0)\,u_2(t), \quad (7a)$$

Fig. 3 Time t dependence of functions $s_1(t)$, $i_1(t)$ and $r_1(t)$ for $\beta = 0.56$ and $\gamma = 0.2$. The parameters are chosen for the COVID-19 outbreak before any population or government reactions came into effect [13]. Thus, they represent the natural COVID-19 outbreak without any control measures within the SIR approach

$$i_2(t) = 1 + \frac{\gamma+\sigma}{\beta}\ln u_2(t) - s_2(0)\,u_2(t), \quad (7b)$$

$$r_2(t) = -\frac{\gamma+\sigma}{\beta}\ln u_2(t)$$
$$- \sigma\int_0^t \mathrm{d}t'\left(1 + \frac{\gamma+\sigma}{\beta}\ln u_2(t') - s_2(0)\,u_2(t')\right), \quad (7c)$$

$$d_2(t) = \sigma\int_0^t \mathrm{d}t'\left(1 + \frac{\gamma+\sigma}{\beta}\ln u_2(t') - s_2(0)\,u_2(t')\right), \quad (7d)$$

$$t = \int_1^{u_2(t)} \frac{\mathrm{d}\xi}{\xi\left(\beta\xi s_2(0) - \beta - (\gamma+\sigma)\ln\xi\right)}. \quad (7e)$$

Solutions for $r_2(t)$ and $d_2(t)$ are obtained by use of Eqs. (2d) and (6c), respectively. Figure 4 depicts exact SIRD solutions for $s_2(t)$, $i_2(t)$, $r_2(t)$ and $d_2(t)$.

In addition, the SIQR model reduces to the SIR model by use of

$$\frac{\mathrm{d}}{\mathrm{d}t}\left(q_3(t) + r_3(t)\right) = \frac{\mathrm{d}}{\mathrm{d}t}r_1(t), \quad (8)$$

changing the index $3 \to 1$ and setting the isolation rate $\delta = 0$. Hence, Eqs. (6a), (6b) and (6d) also hold for the SIQR case if the replacements $\gamma \to \gamma + \delta$, $1 \to 3$ are performed, while Eq. (6c) is a solution for $r_1(t) = q_3(t) + r_3(t)$. Hence, exact solutions are given by

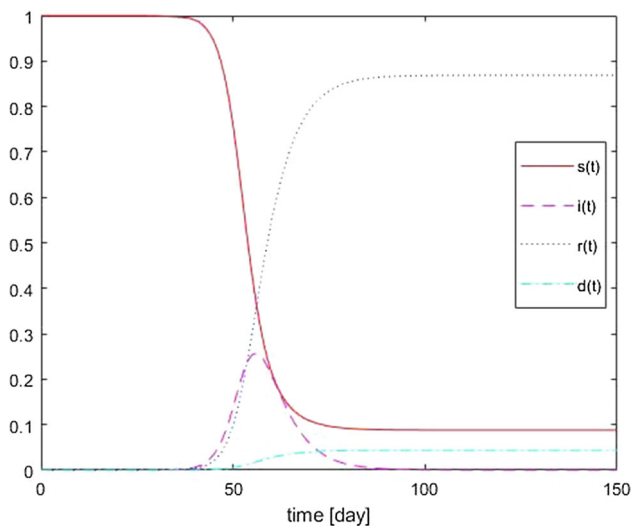$$s_3(t) = s_3(0)\,u_3(t), \quad (9a)$$

Fig. 4 Time t dependence of functions $s_2(t)$, $i_2(t)$, $r_2(t)$ and $d_2(t)$ for $\beta = 0.56$, $\gamma = 0.2$ and $\sigma = 0.01$. The parameters are chosen for the COVID-19 outbreak before any population or government reactions came into effect [13]. Thus, they represent the natural COVID-19 outbreak without any control measures within the SIRD approach

Fig. 5 Time t dependence of functions $s_3(t)$, $i_3(t)$, $q_3(t)$ and $r_3(t)$ for $\beta = 0.56$, $\gamma = 0.2$, $\delta = 0.1$ and $\mu = 0.02$. The parameters are chosen for the COVID-19 outbreak before any population or government reactions came into effect [13]. Thus, they represent the natural COVID-19 outbreak without any control measures within the SIQR approach. The number of isolated individuals reaches its maximum 14 days later in comparison to the peak of infected people

$$i_3(t) = 1 + \frac{\gamma + \delta}{\beta} \ln u_3(t) - s_3(0) u_3(t), \qquad (9b)$$

$$q_3(t) = \delta \int_0^t dt' \, e^{\mu(t'-t)} \\ \times \left(1 + \frac{\gamma + \delta}{\beta} \ln u_3(t') - s_3(0) u_3(t')\right), \qquad (9c)$$

$$r_3(t) = -\frac{\gamma + \delta}{\beta} \ln u_3(t) - \delta \int_0^t dt' \, e^{\mu(t'-t)} \\ \times \left(1 + \frac{\gamma + \delta}{\beta} \ln u_3(t') - s_3(0) u_3(t')\right), \qquad (9d)$$

$$t = \int_1^{u_3(t)} \frac{d\xi}{\xi(\beta\xi s_3(0) - \beta - (\gamma + \delta) \ln \xi)}. \qquad (9e)$$

Solutions for $q_3(t)$ and $r_3(t)$ are obtained by use of Eqs. (3c) and (6c), respectively. Figure 5 depicts exact SIQR solutions for $s_3(t)$, $i_3(t)$, $q_3(t)$ and $r_3(t)$.

Note that the fraction of isolated individuals reaches its maximum later than the fraction of infected individuals. The difference is typically in the order of 10 days.

2.4 Small time limit

Equation (9e) simplifies for small times t since $1 - u_3(t)$ is small in this case. Hence, this evaluation describes the beginning of an outbreak and yields exact short-term
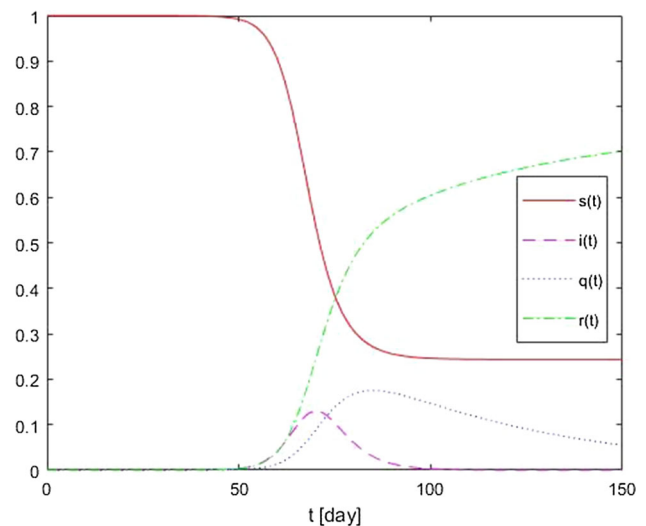
solutions for the SIQR model given by

$$s_3(t) = s_3(0) + \frac{\beta(1 - s_3(0))}{\gamma + \delta - \beta} \left(e^{(\beta-\gamma-\delta)t} - 1\right), \qquad (10a)$$

$$i_3(t) = (1 - s_3(0)) \, e^{(\beta-\gamma-\delta)t}, \qquad (10b)$$

$$q_3(t) = \frac{(1 - s_3(0))\delta}{\beta - \gamma - \delta + \mu} \left(e^{(\beta-\gamma-\delta)t} - e^{-\mu t}\right), \qquad (10c)$$

$$r_3(t) = \frac{(1 - s_3(0))(\gamma + \delta)}{\beta - \gamma - \delta} \left(e^{(\beta-\gamma-\delta)t} - 1\right) \\ - \frac{(1 - s_3(0))\delta}{\beta - \gamma - \delta + \mu} \left(e^{(\beta-\gamma-\delta)t} - e^{-\mu t}\right), \qquad (10d)$$

which also represent short-term solutions for SIR or SIRD models if $r_1(t) = q_3(t) + r_3(t)$ or $q_3(t) = d_2(t)$ is used, indices are changed, i.e. $3 \to 1$ or $3 \to 2$, and vanishing isolation rate $\delta = 0$ or $\delta = \sigma$ is assumed, respectively. By considering Eqs. (10a)–(10d), it is obvious that the short-term behaviour of the epidemic outbreak and its growth rate is controlled by $\beta - \gamma - \delta$ for the three models. Hence, at the start of an epidemic outbreak population and government reactions that lead to negative or at least small but positive $\beta - \gamma - \delta$ are preferable [44].

Remarkably, this fact can also be derived quite trivially by using the fact that at the early stage of an outbreak the number of infected, quarantined and removed individuals is quite small in comparison with the total population number N, i.e. $s_3(t) = 1 - i_3(t) - q_3(t) -$

$r_3(t) = 1 + \mathcal{O}(i_3(t) + q_3(t) + r_3(t))$ and $i_3(t) + q_3(t) + r_3(t) \ll 1$ hold. Thus, Eq. (3b) simplifies to

$$\frac{\mathrm{d}}{\mathrm{d}t} i_3(t) = (\beta - \gamma - \delta) i_3(t), \qquad (11)$$

which also leads to the solution given by Eq. (10b). Note that this approach also holds for time-dependent transmission rate $\beta(t)$ and isolation rate $\delta(t)$, respectively. Hence, Eq. (11) yields

$$i_3(t) = i_3(0) \, \mathrm{e}^{\int_0^t \mathrm{d}t' \, (\beta(t') - \gamma - \delta(t'))} \qquad (12)$$

in this case, which is a generalization of the small time limit given in Eq. (10b).

As an example of the observation that $\beta - \gamma - \delta$ is dominating the early stage of an outbreak, we consider real COVID-19 data from Germany until 28 March 2020 [45]. The first COVID-19 case in Germany was reported on 27 January 2020. However, the number of daily cases was published from 04 March 2020 onwards, i.e. 36 days later. Furthermore, note that data analyses with confirmed cases need to be done carefully due to the delay of 1 to 2 weeks between the calculated and officially recorded number of confirmed cases. Moreover, official reports do not distinguish between infected and isolated individuals. For these reasons, we assume that the number of cases has been recorded from the 45th day of the outbreak and the short-term function $i(t) + q(t)$ given by Eqs. (10b) and (10c) is fitted to real data, where β and δ are determined by the fitting process. The result is depicted in Fig. 6. $\beta = 0.5109$ and $\delta = 0.2007$ are obtained which shows that isolation measures were taken and the transmission rate was reduced in comparison with $\beta = 0.56$ [13]. However, $\beta - \gamma - \delta > 0$ still held which explains the occurrence of the first COVID-19 wave in Germany. Thus, it is clear that a further decreasing transmission rate in combination with a higher isolation rate was needed for stamping out the outbreak. Note that within such an approach the continuous determination [13,46–49] of this rates is a requirement since they show dynamic behaviour while $\beta - \gamma - \delta < 0$ is aimed for.

Remarkably, within this approach, it is not possible to propose a specific intervention during an epidemic outbreak based on this model. However, there are two possible advantages. First, as demonstrated in Fig. 6, the fitting procedure for the early phase of an outbreak yields the transmission and isolation rates β and δ, respectively. Thus, quantitative effects of any interventions on the rates can also be determined. Naturally, interventions only have to take effect individually so that the respective influence can be determined directly. However, since ultimately only the sign of $\beta - \gamma - \delta$ plays a role, this method can be used for measuring the total effect of a number of interventions. Second, in addition to the weighting of the interventions $\beta - \gamma - \delta < 0$ can obviously be aimed for.
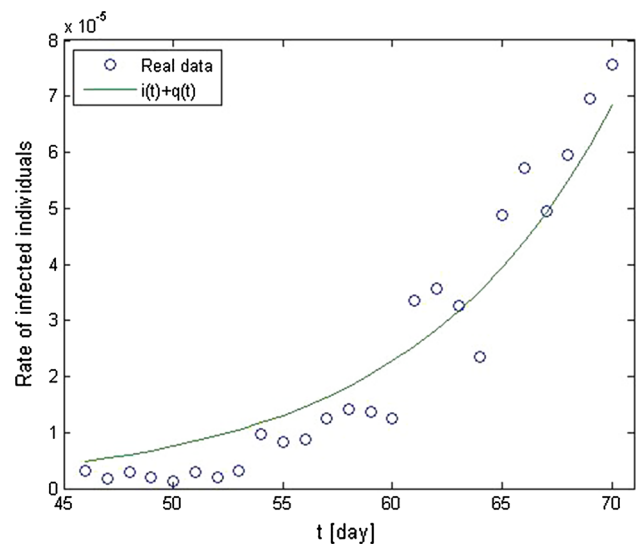

Fig. 6 Short-time behaviour of $i(t) + q(t)$ in comparison with the real data from Germany

2.5 Analysis of daily new cases

The assumption that infected individuals are quarantined leads to a relationship between the number of daily new cases $C(t)$ and infected individuals since considering the incubation period distribution function $\rho(t)$ for quarantining infected people and using the fact that a convolution of this function $\rho(t)$ with $i_3(t)$ describes individuals with starting symptoms leads to

$$c(t) := \frac{C(t)}{N} = \int_{-\infty}^t \mathrm{d}t' \, \rho(t - t') i_3(t'). \qquad (13)$$

Since the incubation period distribution function $\rho(t)$ should be a well-behaved function with just a single peak [50,51], the method of steepest descent [52,53] yields

$$c(t) \simeq i_3(t - \tau) \rho^{\frac{3}{2}}(\tau) \sqrt{\frac{2\pi}{|\rho''(\tau)|}}, \qquad \rho'(\tau) = 0, \quad (14)$$

where τ characterizes the position of the peak of the incubation period distribution function $\rho(t)$ and $\rho''(t)$ is a shorthand notation, i.e. $\rho''(t) = \frac{\mathrm{d}^2\rho(t)}{\mathrm{d}t^2}$. Thus, we find

$$\frac{c(t)}{c(0)} = \frac{i_3(t - \tau)}{i_3(-\tau)}, \qquad (15)$$

which yields

$$c(t) = \frac{c(0) i_3(t - \tau)}{i_3(-\tau)} \qquad (16)$$

for the daily new cases $c(t)$, where $c(0)$ is the initial number of daily cases. Hence, $c(t)$ can be evaluated

by use of the SIQR approach presented in Eq. (9b) for constant transmission rate β and isolation rate δ. In addition, for small times t and time-dependent rates $\beta(t)$ and $\delta(t)$ Eq. (12) yields

$$c(t) = c(0) \, \mathrm{e}^{\int_0^t \mathrm{d}t' \, (\beta(t'-\tau)-\gamma-\delta(t'-\tau))}. \quad (17)$$

Corresponding to this result, daily new cases $c(t)$ were approximated by piecewise exponential functions for the analysis of the first wave of the COVID-19 outbreak [1,54]. In analogy, Eq. (17) can be used for studying the effects of time-dependent transmission (isolation) rate $\beta(t)$ ($\delta(t)$) with regard to the waves of the outbreak.

3 Measure

Lockdowns are widely used as mitigation or suppression strategies during epidemic disease outbreaks. In the analysis presented in the previous Sect. 2.4 it was observed that $\beta - \gamma - \delta$ is the dominant factor at the beginning of an epidemic outbreak. Hence, for the purpose of controlling the spread of an infectious disease decreasing transmission rate β [13] or increasing isolation rate δ is essential since the recovery rate γ is fixed for any given disease. However, the cost of such methodologies has to be taken into account. Replacing β with $(1-\alpha)\beta$ allows the definition of a measure function $m(\alpha,\delta)$ that is used for measuring the lockdown strength. $\alpha = 0$ describes the natural outbreak without any control reactions, while $\alpha = 1$ leads to a vanishing transmission rate and thus describes a total lockdown.

The epidemic peak i_3^* in Eq. (5) is taken as measure function, i.e.

$$m(\alpha,\delta) = 1 + \frac{\gamma+\delta}{(1-\alpha)\beta}$$
$$\times \left(\ln \frac{\gamma+\delta}{(1-\alpha)\beta} - 1 \right), \, m(\alpha,\delta) \geq 0. \quad (18)$$

Within this framework, Fig. 7 illustrates trajectories for which the measure function $m(\alpha,\delta)$ is constant.

Furthermore, a loss function

$$l(\alpha,\delta) = k_1\alpha + k_2\alpha^2 + k_3\frac{\delta^2}{\beta^2} \quad (19)$$

of quadratic form is used for the purpose of measuring the cost of any action the government or the population implements. This specification involves α which describes the strength of measures and the isolation rate δ. Within this approach, the fraction $\frac{\delta}{\beta}$ is considered since it leads to a loss function with arbitrary unit. Remarkably, the total loss includes not only the isolation for every individual but also the cost of organization, management, treatment, cooperation, loss of productivity, etc. Hence, the loss function should be nonlinear. Thus, in this study, a quadratic function Eq.
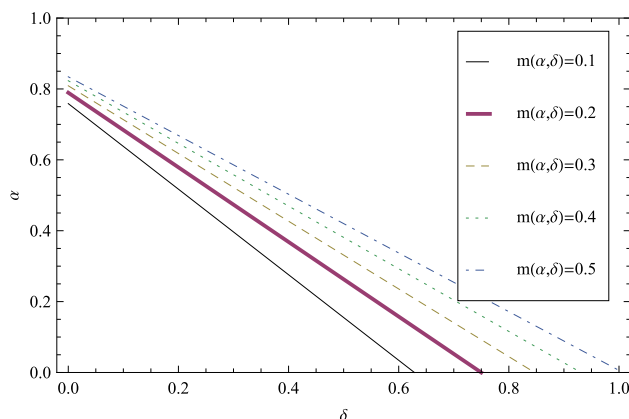

Fig. 7 α in dependence of δ for constant measure $m(\alpha,\delta) = m = 0.1, 0.2, 0.3, 0.4, 0.5$, $\beta = 0.56$ and $\gamma = 0.2$ [13]. The trajectories are described by the linear relationship $\alpha = 1 - \frac{\gamma+\delta}{\beta c}$ between α and δ, where the constant c is connected to the constant value of $m(\alpha,\delta) = m$ by $\mathrm{e}^{m-1} = \left(\frac{c}{\mathrm{e}}\right)^c$

(19) is implemented for estimating quarantine measures as suggested by previous studies about epidemic control [55–57]. Another quite obvious argument for assuming a nonlinear loss function is that there exists no linear relationship between the effects of medical treatment and disease. Note that the loss function $l(\alpha,\delta)$ increases with increasing α or isolation rate δ and $l(\alpha,\delta) \geq 0$ holds as expected. The coefficients k_1, k_2 and k_3 are balancing cost factors due to scales and importance of the three parts in the loss function $l(\alpha,\delta)$. For instance, $k_3 > k_1, k_2$ ($k_1, k_2 > k_3$) suggests that the loss caused by medical treatment (social distancing) is higher than the loss arising from social distancing (medical treatment). Moreover, the relationship between k_1 and k_2 determines whether social distancing contributes more linearly or nonlinearly. If any coefficient is equal to another, this leads to a balanced weighting of the related terms in the loss function in Eq. (19). Within this context, constant values for the loss $l(\alpha,\delta) = l$ are obtained for

$$\alpha = -\frac{k_1}{2k_2} + \frac{\sqrt{\beta^2(k_1^2 + 4k_2l) - 4k_2k_3\delta^2}}{2k_2\beta}$$
$$= -\frac{k_1}{2k_2} + \frac{\sqrt{k_1^2 + 4k_2l}}{2k_2} - \frac{k_3\delta^2}{\beta^2\sqrt{k_1^2 + 4k_2l}} + \mathcal{O}(\delta^4). \quad (20)$$

The minimum of the loss function $l(\alpha,\delta)$ is determined by considering

$$\mathcal{L}(\alpha,\delta,\lambda) = l(\alpha,\delta) - \lambda(m(\alpha,\delta) - m), \quad (21)$$

where λ is a Lagrange multiplier and $m(\alpha,\delta) = m$ a constraint at some level. Thus, considering $\partial_\alpha \mathcal{L}(\alpha,\delta,\lambda) = \partial_\delta \mathcal{L}(\alpha,\delta,\lambda) = \partial_\lambda \mathcal{L}(\alpha,\delta,\lambda) = 0$ yields the optimum trajectory (α^*,δ^*) minimizing the loss function $l(\alpha,\delta)$
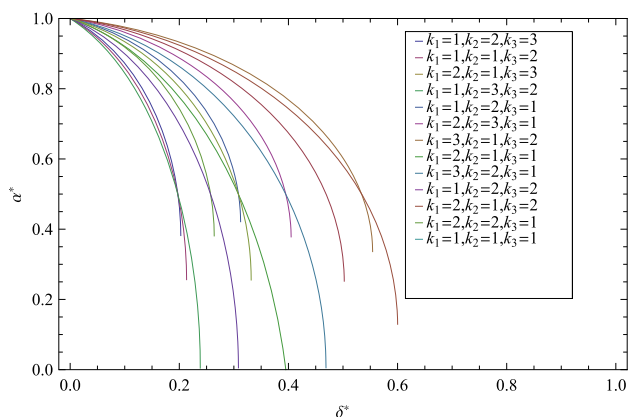
Fig. 8 α^* in dependence of δ^* for $\beta = 0.56$, $\gamma = 0.2$ [13] and varying ratios of k_1, k_2 and k_3

for a given measure function $m(\alpha, \delta)$, i.e.

$$\beta^2 (k_1 + 2\alpha^* k_2)(1 - \alpha^*) = 2k_3 \delta^* (\gamma + \delta^*). \qquad (22)$$

The trajectory is depicted in Fig. 8 for varying ratios of k_1, k_2 and k_3 and described by

$$\alpha^* = \frac{1}{2} - \frac{k_1}{4k_2} + \frac{\sqrt{\beta^2 (k_1 + 2k_2)^2 - 16k_2 k_3 \delta^* (\gamma + \delta^*)}}{4k_2 \beta}$$

$$= 1 - \frac{2k_3 \gamma \delta^*}{\beta^2 (k_1 + 2k_2)} + \mathcal{O}(\delta^{*2}). \qquad (23)$$

Note that within this framework, only solutions $\alpha^* \in [0, 1]$ have to be taken into account.

Due to this analysis, it is observable that lockdown strategies depend on the intent. The epidemic peak is constant for certain values of α and isolation rate δ, as observable in Fig. 7 while other values for the parameters depicted in Fig. 8 have to be chosen if the aim is governed by fears of loss. Remarkably, a total lockdown with $\alpha = 1$ is obviously not the best strategy. A constant epidemic peak is not achievable with this ansatz while the loss is only minimized with this approach if no quarantine measures are taken at all, i.e. isolation rate $\delta^* = 0$. In contrast, increasing δ^* leads to decreasing α^*. The minimum loss on the trajectory (23) lies at position

$$\alpha^* = \frac{1}{2} - \frac{k_1}{4k_2}, \qquad \delta^* = -\frac{\gamma}{2} + \sqrt{\frac{\gamma^2}{4} + \frac{\beta^2 (k_1 + 2k_2)^2}{16k_2 k_3}} \qquad (24)$$

and is described by

$$l(\alpha^*, \delta^*) = \frac{k_1}{2} - \frac{k_1^2}{8k_2} + \frac{k_2}{2} + \frac{k_3 \gamma}{\beta^2}$$

$$\times \left(\frac{\gamma}{2} - \sqrt{\frac{\gamma^2}{4} + \frac{\beta^2 (k_1 + 2k_2)^2}{16k_2 k_3}} \right). \qquad (25)$$

This analysis shows that a lockdown, which is described by $\alpha^* \leq \frac{1}{2}$, is quite sufficient for an optimized epidemic containment strategy that minimizes social costs if a corresponding isolation rate δ^* depending on β, γ, k_1, k_2 and k_3 is provided.

This procedure can be combined with the stamping out strategy presented in Sect. 2.4. It was shown that an optimized strategy can be obtained by lowering the transmission rate β to $\frac{\beta}{2}$ at maximum. The transmission rate should not be lowered further (with regard to the assumptions and models presented in this study). In contrast the isolation rate δ needs to be increased in such a case such that the sign of $\beta - \gamma - \delta$ is negative.

4 Conclusions

Exact solutions of SIRD and SIQR models were presented. In particular, short-term solutions were derived. Results show that an epidemic outbreak is dominated by $\beta - \gamma - \delta$ at its early stage. This is of major interest since β and δ can be modified by government or population reactions. Thus, a stamp out strategy for the epidemic can be used by generating negative $\beta - \gamma - \delta$. The comparison of the analytical approach with real data from Germany indicates that this strategy was not pursued in Germany at the early stage of the COVID-19 pandemic.

In addition, optimizing strategies for choosing α and isolation rate δ were developed. One strategy leads to a constant epidemic peak i_3^*, while another methodology minimizes the social loss function $l(\alpha, \delta)$ for particular values of α and isolation rate δ. Accordingly, choosing the correct strategy depends on the intended purpose. One can try to stamp out the epidemic, reduce the epidemic peak or mitigate the social consequences of measures. In any case, it turns out that a complete lockdown with $\alpha = 1$ is not a reasonable alternative. Contrarily, regardless of the parameters $\alpha \leq \frac{1}{2}$ is obtained if the loss is minimized which indicates that well-chosen containment strategies far away from a complete lockdown are achievable.

Furthermore, the methodology with regard to minimizing the loss function presented in this study should be considered as a first step. The implementation of time t dependent transmission rate $\beta(t)$ and isolation rate $\delta(t)$ is an important possible extension which might lead to additional further insights for epidemic containment strategies.

Note that future research might thematise the incorporation of an input variable describing the proportion of vaccinated residents in a population which may improve the models further. Moreover, such an extension might be of interest for autoregressive models which might also use machine learning techniques [58]. Another open question is the uncertainty in the predictions. Markov chain Monte Carlo (MCMC) methods can be utilized for describing the stochastic behaviour of transitions between the compartmental populations. Moreover, compartmental models can be combined

with deep learning models to predict several epidemic peaks based on the date of previous peaks and uncover hidden interconnections [59,60]. The incorporation of spatial and temporal aspects to the dynamics of epidemic outbreaks is also of great interest. Self-organizing neural networks and fuzzy fractal approaches were proposed as a possible methodology for this purpose [61]. Furthermore, construction of models that can describe both government actions and individual reactions in combination with the influence of weather is of major relevance.

Author contribution statement

The author confirms sole responsibility for the following: study conception and design, data collection, analysis and interpretation of results, and manuscript preparation.

Data Availability Not applicable.

Declarations

Conflict of interest The authors declare that they have no conflict of interest.

References

1. John Hopkins University: Coronavirus Resource Center. Coronavirus COVID-19 global cases. https://coronavirus.jhu.edu/map.html
2. R. Ross, An application of the theory of probabilities to the study of a priori pathometry.–Part I. Proc. Royal Soc. A Math. Phys. Eng. Sci. **92**(638), 204 (1916). https://doi.org/10.1098/rspa.1916.0007
3. R. Ross, H.P. Hudson, An application of the theory of probabilities to the study of a priori pathometry.–Part III. Proc. Royal Soc. A Math. Phys. Eng. Sci. **93**(650), 212 (1917). https://doi.org/10.1098/rspa.1917.0014
4. R. Ross, H.P. Hudson, An application of the theory of probabilities to the study of a priori pathometry.–Part II. Proc. Royal Soc. A Math. Phys. Eng. Sci. **93**(650), 225 (1917). https://doi.org/10.1098/rspa.1917.0014
5. W.O. Kermack, A.G. McKendrick, A contribution to the mathematical theory of epidemics. Proc. Royal Soc. A Math. Phys. Eng. Sci. **115**(772), 700 (1927). https://doi.org/10.1098/rspa.1927.0118
6. H.W. Hethcote, The Mathematics of Infectious Diseases. SIAM Rev. **42**(4), 599 (2006). https://doi.org/10.1137/S0036144500371907
7. R.M. Anderson, R.M. May, Directly transmitted infections diseases: control by vaccination. Science **215**(4536), 1053 (1982). https://doi.org/10.1126/science.7063839
8. H. Hethcote, M. Zhien, L. Shengbing, Effects of quarantine in six endemic models for infectious diseases. Math. Biosci. **180**(1—-2), 141 (2002). https://doi.org/10.1016/S0025-5564(02)00111-6
9. O. Krylova, D.J.D. Earn, Effects of the infectious period distribution on predicted transitions in childhood disease dynamics. J. R. Soc. Interf. **10**(84), 98 (2013). https://doi.org/10.1098/rsif.2013.0098
10. D. He, J. Dushoff, T. Day, J. Ma, D.J.D. Earn, Inferring the causes of the three waves of the 1918 influenza pandemic in England and Wales. Proc. Royal Soc. B Biol. Sci. **280**(1766), 1345 (2013). https://doi.org/10.1098/rspb.2013.1345
11. N.M. Linton, T. Kobayashi, Y. Yang, K. Hayashi, A.R. Akhmetzhanov, S.M. Jung, B. Yuan, R. Kinoshita, H. Nishiura, Incubation Period and Other Epidemiological Characteristics of 2019 Novel Coronavirus Infections with Right Truncation: A Statistical Analysis of Publicly Available Case Data. J. Clin. Med. **9**(2), 538 (2020). https://doi.org/10.3390/jcm9020538
12. Y. Liu, R.M. Eggo, A.J. Kucharski, Secondary attack rate and superspreading events for SARS-CoV-2. The Lancet **395**(10227), 47 (2020). https://doi.org/10.1016/S0140-6736(20)30462-1
13. Y. Öz, A Theoretical model to investigate the influence of temperature, reactions of the population and the government on the COVID-19 outbreak in Turkey, Disaster Medicine and Public Health **16**(1), 214 (2022). https://doi.org/10.1017/dmp.2020.322
14. G.C. Calafiore, C. Novara, C. Possieri, A time-varying SIRD model for the COVID-19 contagion in Italy. Annu. Rev. Control. **50**, 361 (2020). https://doi.org/10.1016/j.arcontrol.2020.10.005
15. S.B. Bastos, D.O. Cajueiro, Modeling and forecasting the early evolution of the Covid-19 pandemic in Brazil. Sci. Rep. **10**, 19457 (2020). https://doi.org/10.1038/s41598-020-76257-1
16. M. Kröger, R. Schlickeiser, Analytical solution of the SIR-model for the temporal evolution of epidemics. Part A: Time-Independent Reproduc. Factor J. Phys. A Math. Theor. **53**(50), 505601 (2020). https://doi.org/10.1088/1751-8121/abc65d
17. K.S. Nisar, S. Ahmad, A. Ullah, K. Shah, H. Alrabaiah, M. Arfan, Mathematical analysis of SIRD model of COVID-19 with Caputo fractional derivative based on real data. Results Phys. **21**, 103772 (2021). https://doi.org/10.1016/j.rinp.2020.103772
18. D. Sen, D. Sen, Use of a modified SIRD model to analyze COVID-19 data. Indust. Eng. Chem. Res. **60**(11), 4251 (2021). https://doi.org/10.1021/acs.iecr.0c04754
19. R. Schlickeiser, M. Kröger, Analytical solution of the SIR-model for the temporal evolution of epi-

demics: part B Semi-time case. J. Phys. A: Math. Theor. **54**(17), 175601 (2021). https://doi.org/10.1088/1751-8121/abed66

20. V. Martinez, A modified SIRD model to study the evolution of the COVID-19 pandemic in Spain. Symmetry **13**(4), 723 (2021). https://doi.org/10.3390/sym13040723

21. E. Estrada, COVID-19 and SARS-CoV-2, modeling the present, looking at the future. Phys. Rep. **869**, 1 (2020). https://doi.org/10.1016/j.physrep.2020.07.005

22. Y. Liu, A.A. Gayle, A. Wilder-Smith, J. Rocklöv, The reproductive number of COVID-19 is higher compared to SARS coronavirus. J. Travel Med. **27**(2), 1 (2020). https://doi.org/10.1093/jtm/taaa021

23. M. D'Arienzoa, A. Coniglio, Assessment of the SARS-CoV-2 basic reproduction number, $\mathcal{R}_0$, based on the early phase of COVID-19 outbreak in Italy. Biosafety Health **2**(2), 57 (2020). https://doi.org/10.1016/j.bsheal.2020.03.004

24. C. Anastassopoulou, L. Russo, A. Tsakris, C. Siettos, Data-based analysis, modelling and forecasting of the COVID-19 outbreak. PLoS ONE **15**(3), 0230405 (2020). https://doi.org/10.1371/journal.pone.0230405

25. D. Fanelli, F. Piazza, Analysis and forecast of COVID-19 spreading in China. Italy and France, Chaos, Solitons & Fractals **134**, 109761 (2020). https://doi.org/10.1016/j.chaos.2020.109761

26. N. Qualls, A. Levitt, N. Kanade, N. Wright-Jegede, S. Dopson, M. Biggerstaff, C. Reed, A. Uzicanin, Community mitigation guidelines to prevent pandemic influenza – United States, 2017. Recommend. Rep. I **66**(1), 1 (2017). https://doi.org/10.15585/mmwr.rr6601a1externalicon

27. M.F. Liew, W.T. Siow, G. MacLaren, K.C. See, Preparing for COVID-19: early experience from an intensive care unit in Singapore. Crit. Care **24**, 83 (2020). https://doi.org/10.1186/s13054-020-2814-x

28. L. Stone, B. Shulgin, Z. Agur, Theoretical examination of the pulse vaccination policy in the SIR epidemic model. Math. Comput. Model. **31**(4–5), 207 (2000). https://doi.org/10.1016/S0895-7177(00)00040-6

29. A. Korobeinikov, Lyapunov functions and global stability for SIR and SIRS epidemiological models with nonlinear transmission. Bull. Math. Biol. **68**(3), 615 (2006). https://doi.org/10.1007/s11538-005-9037-9

30. G. Huang, Y. Takeuchi, W. Ma, D. Wei, Global stability for delay SIR and SEIR epidemic models with nonlinear incidence rate. Bull. Math. Biol. **72**(5), 1192 (2010). https://doi.org/10.1007/s11538-009-9487-6

31. C. Ji, D. Jiang, Threshold behaviour of a stochastic SIR model. Appl. Math. Model. **38**(21–22), 5067 (2014). https://doi.org/10.1016/j.apm.2014.03.037

32. Y.-C. Chen, P.-E. Lu, C.-S. Chang, T.-H. Liu, A time-dependent SIR model for COVID-19 with undetectable infected persons. IEEE Trans. Netw. Sci. Eng. **7**(4), 3279 (2020). https://doi.org/10.1109/TNSE.2020.3024723

33. I. Cooper, A. Mondal, C.G. Antonopoulos, A SIR model assumption for the spread of COVID-19 in different communities. Chaos, Solitons Fractals **139**, 110057 (2020). https://doi.org/10.1016/j.chaos.2020.110057

34. P. Wang, J. Jia, Stationary distribution of a stochastic SIRD epidemic model of Ebola with double saturated incidence rates and vaccination. Adv. Differ. Equ. **2019**, 433 (2019). https://doi.org/10.1186/s13662-019-2352-5

35. M. Al-Raeei, The forecasting of COVID-19 with mortality using SIRD epidemic model for the United States, Russia, China, and the Syrian Arab Republic. AIP Adv. **10**(6), 065325 (2020). https://doi.org/10.1063/5.0014275

36. A. Sedaghat, F. Alkhatib, N. Mostafaeipour, S.A.A. Oloomi, Prediction of COVID-19 dynamics in Kuwait using SIRD model. Integr. J. Med. Sci. **7**, 170 (2020). https://doi.org/10.15342/ijms.7.170

37. L.-I. Wu, Z. Feng, Homoclinic bifurcation in an $SIQR$ model for childhood diseases. J. Differ. Equ. **168**(1), 150 (2000). https://doi.org/10.1006/jdeq.2000.3882

38. M. Erdem, M. Safan, C. Castillo-Chavez, Mathematical analysis of an SIQR influenza model with imperfect quarantine. Bull. Math. Biol. **79**(7), 1612 (2017). https://doi.org/10.1007/s11538-017-0301-6

39. Q. Liu, D. Jiang, N. Shi, Threshold behavior in a stochastic SIQR epidemic model with standard incidence and regime switching. Appl. Math. Comput. **316**, 310 (2018). https://doi.org/10.1016/j.amc.2017.08.042

40. A. Tiwari, Modelling and analysis of COVID-19 epidemic in India. J. Safety Sci. Resilience **1**(2), 135 (2020). https://doi.org/10.1016/j.jnlssr.2020.11.005

41. J.C. Miller, A Note on the Derivation of Epidemic Final Sizes. Bull. Math. Biol. **74**(9), 2125 (2012). https://doi.org/10.1007/s11538-012-9749-6

42. T. Harko, F.S.N. Lobo, M.K. Mak, Exact analytical solutions of the Susceptible-Infected-Recovered (SIR) epidemic model and of the SIR model with equal death and birth rates. Appl. Math. Comput. **236**, 184 (2014). https://doi.org/10.1016/j.amc.2014.03.030

43. J.C. Miller, Mathematical models of SIR disease spread with combined non-sexual and sexual transmission routes. Infect. Disease Modell. **2**(1), 35 (2017). https://doi.org/10.1016/j.idm.2016.12.003

44. H. Tomaskova, E.B. Tirkolaee, Using a Process Approach to Pandemic Planning: A Case Study. Appl. Sci. **11**(9), 4121 (2021). https://doi.org/10.3390/app11094121

45. Robert Koch Institute: Infectious Diseases. Coronavirus Disease 2019 (COVID-19) - Situation Report of the Robert Koch Institute. https://www.rki.de/EN/Content/infections/epidemiology/outbreaks/COVID-19/Situationsberichte_Tab.html

46. P. Wu, X. Hao, E.H.Y. Lau, J.Y. Wong, K.S.M. Leung, J.T. Wu, B.J. Cowling, G.M. Leung, Real-time tentative assessment of the epidemiological characteristics of novel coronavirus infections in Wuhan, China, as at 22 January 2020. Eurosurveillance **25**(3), 2000044 (2020). https://doi.org/10.2807/1560-7917.ES.2020.25.3.2000044

47. H. Nishiura, T. Kobayashi, Y. Yang, K. Hayashi, T. Miyama, R. Kinoshita, N.M. Linton, S.M. Jung, B. Yuan, A. Suzuki, A.R. Akhmetzhanov, The Rate of Underascertainment of Novel Coronavirus (2019-nCoV) Infection: Estimation Using Japanese Passengers Data on Evacuation Flights. J. Clin. Med. **9**(2), 419 (2020). https://doi.org/10.3390/jcm9020419

48. R.A. Neher, R. Dyrdak, V. Druelle, E.B. Hodcroft, J. Albert, Potential impact of seasonal forcing on a SARS-

CoV-2 pandemic. Swiss Med. Wkly. **150**, 1112 (2020). https://doi.org/10.4414/smw.2020.20224

49. Q. Li, X. Guan, P. Wu, X. Wang, L. Zhou, Y. Tong, R. Ren, K.S.M. Leung, E.H. Lau, J.Y. Wong, X. Xing, N. Xiang, Y. Wu, C. Li, Q. Chen, D. Li, T. Liu, J. Zhao, M. Liu, W. Tu, C. Chen, L. Jin, R. Yang, Q. Wang, S. Zhou, R. Wang, H. Liu, Y. Luo, Y. Liu, G. Shao, H. Li, Z. Tao, Y. Yang, Z. Deng, B. Liu, Z. Ma, Y. Zhang, G. Shi, T.T.Y. Lam, J.T. Wu, G.F. Gao, B.J. Cowling, B. Yang, G.M. Leung, Z. Feng, Early Transmission Dynamics in Wuhan, China, of Novel Coronavirus-Infected Pneumonia. N. Engl. J. Med. **382**(13), 1199 (2020). https://doi.org/10.1056/NEJMoa2001316

50. J.A. Backer, D. Klinkenberg, J. Wallinga, Incubation period of 2019 novel coronavirus (2019-nCoV) infections among travellers from Wuhan, China, 20–28 January 2020. Eurosurveillance **25**(5), 2000062 (2020). https://doi.org/10.2807/1560-7917.ES.2020.25.5.2000062

51. X. He, E.H.Y. Lau, P. Wu, X. Deng, J. Wang, X. Hao, Y.C. Lau, J.Y. Wong, Y. Guan, X. Tan, X. Mo, Y. Chen, B. Liao, W. Chen, F. Hu, Q. Zhang, M. Zhong, Y. Wu, L. Zhao, F. Zhang, B.J. Cowling, F. Li, G.M. Leung, Temporal dynamics in viral shedding and transmissibility of COVID-19. Nat. Med. **26**(5), 672 (2020). https://doi.org/10.1038/s41591-020-0869-5

52. P. Debye, Näherungsformeln für die Zylinderfunktionen für große Werte des Arguments und unbeschränkt veränderliche Werte des Index. Math. Ann. **67**(4), 535 (1909). https://doi.org/10.1007/BF01450097

53. P. Deift, X. Zhou, A steepest descent method for oscillatory Riemann-Hilbert problems, Asymptotics for the MKdV equation. Ann. Math. **137**(2), 295 (1993). https://doi.org/10.2307/2946540

54. N. Crokidakis, COVID-19 spreading in Rio de Janeiro, Brazil: Do the policies of social isolation really work? Chaos, Solitons Fractals **136**, 109930 (2020). https://doi.org/10.1016/j.chaos.2020.109930

55. D. Kirschner, S. Lenhart, S. Serbin, Optimal control of the chemotherapy of HIV. J. Math. Biol. **35**(7), 775 (1997). https://doi.org/10.1007/s002850050076

56. M.A.L. Caetano, T. Yoneyama, Optimal and suboptimal control in dengue epidemics. Optimal Control: Appl. Methods **22**(2), 63 (2001). https://doi.org/10.1002/oca.683

57. E. Jung, S. Lenhart, Z. Feng, Optimal control of treatments in a two-strain tuberculosis model. Discr. Continu. Dyn. Syst. B **2**(4), 473 (2002). https://doi.org/10.3934/dcdsb.2002.2.473

58. B. Lucas, B. Vahedi, M. Karimzadeh, A spatiotemporal machine learning approach to forecasting COVID-19 incidence at the county level in the USA. Int. J. Data Sci. Anal. (2022). https://doi.org/10.1007/s41060-021-00295-9

59. Q. Deng, Dynamics and Development of the COVID-19 Epidemic in the United States: A Compartmental Model Enhanced With Deep Learning Techniques. J. Med. Internet Res. **22**(8), 21173 (2020). https://doi.org/10.2196/21173

60. T. Šušterčič, A. Blagojević, D. Cvetković, A. Cvetković, I. Lorencin, S.B. Šegota, D. Milovanović, D. Baskić, Z. Car, N. Filipović, Epidemiological Predictive Modeling of COVID-19 Infection: Development, Testing, and Implementation on the Population of the Benelux Union, Frontiers in Public. Health **9**, 727274 (2021). https://doi.org/10.3389/fpubh.2021.727274

61. P. Melin, O. Castillo, Spatial and Temporal Spread of the COVID-19 Pandemic Using Self Organizing Neural Networks and a Fuzzy Fractal Approach. Sustainability **13**(15), 8295 (2021). https://doi.org/10.3390/su13158295